

CONSTRAINTS ON TWO ACTIVE GALACTIC NUCLEI IN THE MERGER REMNANT COSMOS J100043.15+020637.2

J. M. WROBEL^{1,2}, J. M. COMERFORD³, AND E. MIDDELBERG⁴

Accepted by ApJ on 2014 January 15

ABSTRACT

COSMOS J100043.15+020637.2 is a merger remnant at $z = 0.36$ with two optical nuclei, NW and SE, offset by 500 mas (2.5 kpc). Prior studies suggest two competing scenarios for these nuclei: (1) SE is an active galactic nucleus (AGN) lost from NW due to a gravitational-wave recoil. (2) NW and SE each contain an AGN, signaling a gravitational-slingshot recoil or inspiralling AGNs. We present new images from the Very Large Array (VLA) at a frequency $\nu = 9.0$ GHz and a FWHM resolution $\theta = 320$ mas (1.6 kpc), and the Very Long Baseline Array (VLBA) at $\nu = 1.52$ GHz and $\theta = 15$ mas (75 pc). The VLA imaging is sensitive to emission driven by AGNs and/or star formation, while the VLBA imaging is sensitive only to AGN-driven emission. No radio emission is detected at these frequencies. Folding in prior results, we find: (a) The properties of SE and its adjacent X-ray feature resemble those of the unobscured AGN in NGC 4151, albeit with a much higher narrow emission-line luminosity. (b) The properties of NW are consistent with it hosting a Compton-thick AGN that warms ambient dust, photoionizes narrow emission-line gas and is free-free absorbed by that gas. Finding (a) is consistent with scenarios (1) and (2). Finding (b) weakens the case for scenario (1) and strengthens the case for scenario (2). Follow-up observations are suggested.

Subject headings: galaxies: active — galaxies: individual (COSMOS J100043.15+020637.2) — galaxies: interactions — galaxies: nuclei

1. MOTIVATION

Simulations suggest that galaxy mergers can produce remnants with two or more massive black holes (Hoffman & Loeb 2007; Amaro-Seoane et al. 2010; Kulkarni & Loeb 2012). When these black holes accrete, they can appear as two or more active galactic nuclei (AGNs) on kiloparsec scales (Van Wassenhove et al. 2012; Blecha et al. 2013b). Systematic surveys for such multiple AGNs could provide observational constraints on AGN activation and tidally enhanced star formation (e.g., Liu et al. 2012; Koss et al. 2012), and on the black hole merger rate, with consequences for the signals expected for pulsar timing arrays and gravity-wave detectors (Hobbs et al. 2010; Dotti et al. 2012). Guided by early serendipitous discoveries of dual AGNs like 3C 75 (Owen et al. 1985) and NGC 6240 (Beswick et al. 2001; Komossa et al. 2003; Gallimore & Beswick 2004), recent systematic surveys are now yielding spectroscopic samples of dual AGN candidates (e.g., Comerford et al. 2009a; Wang et al. 2009; Liu et al. 2010; Smith et al. 2010; Koss et al. 2012; Barrows et al. 2013; Comerford et al. 2013).

Candidate dual AGNs can be difficult to confirm due to obscuration and resolution issues (Comerford et al. 2011; Fu et al. 2011a; Shen et al. 2011; Fu et al. 2012;

Comerford et al. 2012). Moreover, some candidates may turn out to be imposters because they harbor a recoiling AGN, a situation that both complicates and enriches matters (e.g., Blecha et al. 2011; Guedes et al. 2011; Eracleous et al. 2012). This paper focuses on one such case, COSMOS J100043.15+020637.2 (J1000+0206 hereafter). Early reports on J1000+0206 (Smolcic et al. 2008; Elvis 2009; Comerford et al. 2009b; Civano et al. 2010) were prompted by its unusual optical nature, involving two apparent nuclei in a merger remnant with a tidal tail (Scoville et al. 2007).

The integrated optical emission-line redshift of J1000+0206 is $z = 0.36$ (Lilly et al. 2007). Adopting the nomenclature and cosmology⁵ of Civano et al. (2012), the two nuclei, SE and NW, have a projected separation of 500 mas (2.5 kpc). Two scenarios have emerged for these optical nuclei: either NW and SE each contain an AGN with its own narrow emission-line region, or SE is an AGN recoiling from NW due to the asymmetric emission of gravitational waves during black-hole coalescence. Hydrodynamic simulations, with radiative transfer calculations, of a gas-rich major merger show that each scenario is consistent with available data (Blecha et al. 2013a).

Smolcic et al. (2008) assumed that the emission from J1000+0206 at a frequency $\nu = 1.4$ GHz (Schinnerer et al. 2007) is driven by its spectroscopically-identified AGN. But this is far from certain. Figure 1 shows that the radio emission is localized to the inner portions of the merger remnant (Schinnerer et al. 2007, 2010), where simulations indicate that star formation can occur (Blecha et al. 2013a). Also, Civano et al. (2012) recently discovered an extended X-ray feature offset by

¹ National Radio Astronomy Observatory, P.O. Box O, Socorro, NM 87801; jwrobel@nrao.edu

² The National Radio Astronomy Observatory (NRAO) is a facility of the National Science Foundation, operated under cooperative agreement by Associated Universities, Inc.

³ Department of Astrophysical and Planetary Sciences, University of Colorado, Boulder, CO 80309; julie.comerford@colorado.edu

⁴ Astronomisches Institut, Ruhr-Universität Bochum, Universitätsstr. 150, 44801, Bochum, Germany; middelberg@astro.rub.de

⁵ $H_0 = 70 \text{ km s}^{-1} \text{ Mpc}^{-1}$, $\Omega_M = 0.3$, $\Omega_\Lambda = 0.7$

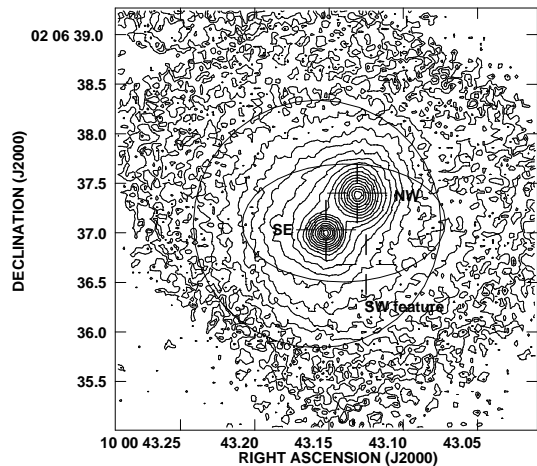


FIG. 1.— HST/ACS image of the F814W emission from J1000+0206 spanning $4.2''$. The plus signs mark the positions and 3σ astrometric errors of the SE and NW optical nuclei (Scoville et al. 2007), and the approximate position of the X-ray feature offset by about 500 mas to the SW of SE (Civano et al. 2012). The circle and ellipse are derived from VLA images at $\nu = 1.4$ GHz with $\theta = 2.5''$ and $1.5''$, respectively (Schinnerer et al. 2010). A point-like source was detected in the former image, and the circle shows its localization as $\theta = 2.5''$. A resolved source was detected in the latter image, and the ellipse shows its deconvolved Gaussian extent at FWHM of $2.05'' \times 1.19''$ with an elongation position angle PA = 91° . Scale is $1'' = 5.03$ kpc.

about 500 mas (2.5 kpc) to the southwest (SW) of the SE optical nucleus, further complicating the observational picture.

If the radio emission from J1000+0206 arises from the AGNs and star formation, Figure 1 makes it clear that disentangling these contributions requires imaging at subarcsecond resolution. § 2 presents new images from the Karl G. Jansky Very Large Array (VLA; Perley et al. 2011) at $\nu = 9.0$ GHz and a FWHM resolution $\theta = 320$ mas (1.6 kpc), and from the Very Long Baseline Array (VLBA; Napier et al. 1994) at $\nu = 1.5$ GHz and $\theta = 15$ mas (75 pc). § 3 explores the implications of the new imaging, while a summary and conclusions appear in § 4.

2. IMAGING

2.1. VLA

J1000+0206 was observed with the VLA in its A configuration on 2012 October 12 UT under proposal code 12B-072. A coordinate equinox of 2000 was used. J1024-0052, with a one-dimensional position error of 10 mas (1σ), was employed as a phase calibrator. The switching time between it and J1000+0206 was 480 s, and involved a switching angle of 6.6° . The *a priori* pointing position for J1000+0206 was shifted $0.6''$ south of the SDSS position (Comerford et al. 2009b) to avoid the risk of phase-center artifacts. Every 1 s the correlator produced 1024 contiguous 2-MHz channels, yielding a total bandwidth of 2.048 GHz per circular polarization centered at $\nu = 9.0$ GHz. Observations of 3C 138 were used to set the amplitude scale to an accuracy of about 1% (Perley & Butler 2013). The net exposure time on J1000+0206 was about 2150 s.

Release 4.1.0 of the Common Astronomy Software Applications (CASA) package (McMullin et al. 2007) was used to calibrate and edit the data in an automated fash-

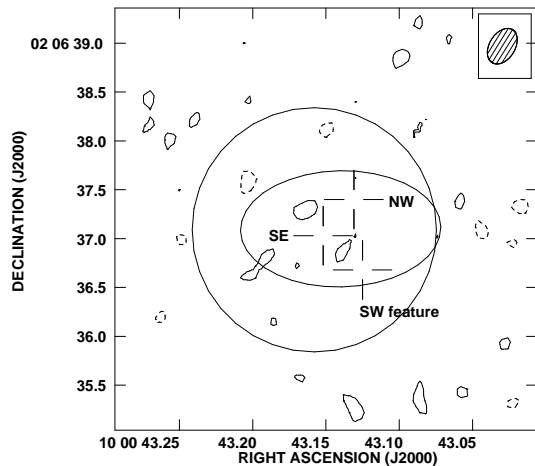


FIG. 2.— VLA image of Stokes I emission from J1000+0206 at $\nu = 9.0$ GHz and spanning $4.2''$. The rms noise is 0.006 mJy beam $^{-1}$ (1σ) and the beam dimensions at FWHM are 400 mas \times 260 mas with an elongation PA = -32° (boxed hatched ellipse). Contours are at $-6, -4, -2, 2, 4$, and 6 times 1σ . Negative contours are dashed and positive ones are solid. No emission was detected above 3σ . The circle, ellipse, plus signs and scale are the same as for Fig. 1.

ion⁶. After further minor edits, the CASA task *imager* was used to form and deconvolve a naturally-weighted image of the Stokes I emission from J1000+0206. This imaged spans 2561×60 mas in each coordinate, has an rms noise level $\sigma = 0.006$ mJy beam $^{-1}$ and a geometric resolution at FWHM $\theta = 320$ mas. Its inner portions are shown in Figure 2. With adequate signal-to-noise, structures as large as about $10\theta \sim 3.2''$ could be represented in Figure 2. No emission was detected above a threshold of 0.018 mJy beam $^{-1}$ (3σ).

2.2. VLBA

J1000+0206 was observed with the VLBA during four 6-hour sessions spanning 2012 June 24 to 2013 January 11 under proposal code BM360. A coordinate equinox of 2000 was used. J1011+0106, with a one-dimensional position error of 2 mas (1σ), was used as a phase calibrator. The switching time between it and J1000+0206 was 360 s, and involved a switching angle of 2.7° . Every 4.1 s the correlator (Deller et al. 2011) produced 128 contiguous 2-MHz channels, yielding a total bandwidth of 0.256 GHz per circular polarization centered at $\nu = 1.52$ GHz. VLBA system temperatures and gains were used to set the amplitude scale to an accuracy of about 5%. A total of about 450 baseline hours were accrued on J1000+0206.

For each 6-hour session, NRAO's Astronomical Image Processing System (AIPS; Greisen 2003) was used to calibrate and edit the data following the approach described by Middelberg et al. (2013). The AIPS task *imager* was used to form and deconvolve a naturally-weighted image of the Stokes I emission from J1000+0206. This image spans 2048×1 mas in each coordinate, has a geometric resolution at FWHM $\theta = 15$ mas, and was corrected for primary beam attenuation. Combining the *u-v* data from the four sessions resulted in an rms noise level $\sigma = 0.013$ mJy beam $^{-1}$. With adequate signal-to-noise, structures as large as about $10\theta \sim 150$ mas could

⁶ science.nrao.edu/facilities/vla/data-processing/pipeline

be imaged. No emission was detected above a threshold of $0.078 \text{ mJy beam}^{-1}$ (6σ).

3. IMPLICATIONS

3.1. Overview

The new VLBA image at $\nu = 1.52 \text{ GHz}$ and $\theta = 15 \text{ mas}$ (75 pc) filters for emission with a rest-frame brightness temperature $T_b > 3.5 \times 10^5 \text{ K}$, not achieved by even the most compact starbursts (Condon 1992). Moreover, the VLBA image is too shallow to detect even the most luminous radio supernova beyond $z \sim 0.1$ (e.g., Garrett et al. 2005; Middelberg et al. 2013). Thus the VLBA image is insensitive to emission driven by star formation. In contrast, the new VLA image (Figure 2) at $\nu = 9.0 \text{ GHz}$ and $\theta = 320 \text{ mas}$ (1.6 kpc) is sensitive to emission driven by star formation, and to AGN-driven emission in the SE or NW optical nuclei or associated with the X-ray feature offset to the SW of the SE optical nucleus (Comerford et al. 2009b; Civano et al. 2010, 2012).

Applying a K-correction for a spectral index $\alpha = -0.7$ ($S \propto \nu^\alpha$), the VLA nondetections in Figure 2 imply that on scales of $1 \theta = 0.32''$ (1.6 kpc) to $10 \theta = 3.2''$ (16 kpc) the merger remnant has a spectral luminosity $L_{9.0 \text{ GHz}} < 7.3 \times 10^{21} \text{ W Hz}^{-1}$. Given these sub-galactic scales, we adopt local indicators of star formation rates (SFRs) (e.g., Calzetti 2012). We apply equation (15) of Murphy et al. (2011) at a rest-frame frequency $\nu = 9.0(1+z) \text{ GHz} = 12.2 \text{ GHz}$, include a thermal contribution for an electron temperature $T_e = 10^4 \text{ K}$ and a non-thermal contribution with a spectral index $\alpha = -0.8$, and find a $\text{SFR} < 17 \text{ M}_\odot \text{ yr}^{-1}$ for a Kroupa initial mass function (IMF). This is an interesting regime to be exploring, given that the host galaxies of optically-selected AGNs at $z < 0.3$ could have $\text{SFR} \sim 1\text{--}20 \text{ M}_\odot \text{ yr}^{-1}$, spanning values for normal spiral galaxies to those for moderately luminous starbursts (Kim et al. 2006; Condon et al. 2013).

Prior VLA imaging at $\nu = 1.4 \text{ GHz}$ (Schinnerer et al. 2010) localized the emission to the circular and elliptical regions, outlined in Figures 1 and 2, that encompass the inner merger remnant, the optical nuclei SE and NW, and the X-ray feature SW of the SE nucleus. The circular region marks a point-like source with an integrated flux density $S_{1.4 \text{ GHz}} = 0.113 \pm 0.010 \text{ mJy}$ and a K-corrected spectral luminosity $L_{1.4 \text{ GHz}} \sim 4.6 \times 10^{22} \text{ W Hz}^{-1}$. If driven by star formation only, the corresponding $\text{SFR} = 34 \text{ M}_\odot \text{ yr}^{-1}$ (Murphy et al. 2011, eqn. 15). This is at least a factor of two higher than the new VLA limit derived above, meaning that up to half of the integrated flux density could arise from star formation. Conversely, any AGN-driven emission could have an integrated $S_{1.4 \text{ GHz}} \sim 0.056\text{--}0.113 \text{ mJy}$ and a K-corrected luminosity $\nu L_\nu(1.4 \text{ GHz}) = (3\text{--}6) \times 10^{38} \text{ erg s}^{-1}$, the regime of low-luminosity AGN (LLAGN) at $z = 0$ (Ho 2008).

Analyses of the *HST* F814W ACS image and the Keck/DEIMOS spectrum of the galaxy were reported in Comerford et al. (2009b), and can be summarized as follows. Using Source EXtractor on the *HST* image, the SE and NW optical nuclei were found to be aligned along a $\text{PA} = 139.6^\circ$, with a projected separation of $500 \pm 9 \text{ mas}$ ($2.50 \pm 0.05 \text{ kpc}$). The DEIMOS spectrum was taken with a slit $\text{PA} = 143.3^\circ$ and spanning $4730\text{--}9840 \text{ \AA}$ in wavelength. This spectrum revealed double narrow emission-

line components, with line flux ratios of both components falling within the AGN region of the Baldwin-Phillips-Terlevich diagram, within the 1σ errors on the flux measurements.

Projected spatial separations between the double emission-line components of $2.1 \pm 0.7 \text{ kpc}$, $1.4 \pm 0.6 \text{ kpc}$, and $2.3 \pm 0.6 \text{ kpc}$ were measured for [O III] $\lambda 5007$, H α , and [N II] $\lambda 6584$, respectively. The mean of the three spatial separations measurements, weighted by their inverse variances, is $1.9 \pm 0.4 \text{ kpc}$. However, the H α spatial separation measurement is not consistent with the separations measured in [O III] $\lambda 5007$ and [N II] $\lambda 6584$ and is skewed low because of partial obscuration by an imperfectly subtracted night-sky line. Using only the spatial separations measured in [O III] $\lambda 5007$ and [N II] $\lambda 6584$ (which are consistent with one another, to within the 1σ errors), the inverse-variance-weighted mean spatial separation is $2.2 \pm 0.5 \text{ kpc}$.

In projection, the spatial separation between the double emission-line components ($2.2 \pm 0.5 \text{ kpc}$) is consistent with the spatial separation between the double nuclei in the *HST* image ($2.50 \pm 0.05 \text{ kpc}$), to within their errors. There is a 3.7° difference between the PA of the DEIMOS slit and the PA of the two nuclei in the *HST* image, but this results in a negligible (0.2%) difference between the spectrum-based and image-based measurements of spatial separations. These similar spatial separations, combined with the excitation state of the narrow emission-line components, are taken as strong indicators for the presence of two AGNs, likely associated with SE and NW.

The exposure time of the DEIMOS spectrum was too short to allow us to localize, with confidence, each narrow emission-line component with each optical nucleus. For now we make the plausible assumption that [O III] $\lambda 5007$ luminosities $L([\text{OIII}]) = 4.8\text{--}9.9 \times 10^{42} \text{ erg s}^{-1}$ and excitation ratios $[\text{OIII}]\lambda 5007/\text{H}\beta = 3.4\text{--}4.4$ for the two AGNs (Comerford et al. 2009b). In the near future we will obtain Keck/OSIRIS data to test this important assumption (F. Muller-Sanchez, priv. comm.).

3.2. The SE Optical Nucleus and its SW X-ray Feature

Civano et al. (2010, 2012) provide strong evidence that the SE optical nucleus is an unobscured AGN of Type 1, thus featuring a broad emission-line region. SE has an X-ray counterpart with a luminosity $L(2\text{--}10 \text{ keV}) = 1.14 \times 10^{43} \text{ erg s}^{-1}$ (Civano et al. 2010, 2012). Its Eddington ratio is 0.04 (Civano et al. 2010; Trump et al. 2011), typical for a Type 1 AGN in COSMOS (Trump et al. 2009). The new VLA and VLBA nondetections of SE imply that any AGN-driven emission has K-corrected luminosities $\nu L_\nu(9.0 \text{ GHz}) < 6.6 \times 10^{38} \text{ erg s}^{-1}$ (3σ) on scales below 1.6 kpc and $\nu L_\nu(1.52 \text{ GHz}) < 4.7 \times 10^{38} \text{ erg s}^{-1}$ (6σ) on scales below 75 pc . From § 3.1, the luminosity of any AGN-driven emission from SE cannot exceed $\nu L_\nu(1.4 \text{ GHz}) = 6 \times 10^{38} \text{ erg s}^{-1}$.

Following Terashima & Wilson (2003), the new VLA photometry for SE yields $\log \nu L_\nu(9.0 \text{ GHz})/L(2\text{--}10 \text{ keV}) < -4.2$. This value is consistent with SE's modest Eddington ratio (Ho 2008). From § 3.1, the [O III] $\lambda 5007$ luminosity of SE is $L([\text{OIII}]) = 4.8\text{--}9.9 \times 10^{42} \text{ erg s}^{-1}$ (Comerford et al. 2009b). The VLBA luminosity, free from contamination from star forma-

tion, thus implies that SE is radio quiet as defined by Zakamska et al. (2004) or Trump et al. (2011, 2013), a trait that is also consistent with its modest Eddington ratio.

For context, several key properties of SE resemble or are consistent with those of the prototypical Type 1 AGN NGC 4151. Adopting a distance of 13.3 Mpc for NGC 4151, it has (a) $L(2 - 10 \text{ keV}) = 5.0 \times 10^{42} \text{ erg s}^{-1}$ (Ho 2009); (b) when integrated within a radius of $2''$ (130 pc), $\nu L_\nu(1.425 \text{ GHz}) = 1.0 \times 10^{38} \text{ erg s}^{-1}$, $\nu L_\nu(8.465 \text{ GHz}) = 1.4 \times 10^{38} \text{ erg s}^{-1}$ and $\alpha = -0.75$ (Kukula et al. 1995; Ho & Ulvestad 2001); and (c) $\log \nu L_\nu(8.465 \text{ GHz})/L(2 - 10 \text{ keV}) = -4.6$. Mundell et al. (2003) and Wang et al. (2011a) report evidence that the radio source dynamically interacts with the interstellar medium (ISM) at these radii in NGC 4151.

Civano et al. (2012) noted that the X-ray feature offset by about 500 mas (2.5 kpc) to the SW of the SE optical nucleus could be driven by star formation. Indeed, de La Fuente Marcos & de La Fuente Marcos (2008) suggest that the impulse from the passage of a recoiling black hole could trigger star formation in its wake. In the scenario where SE has recoiled from NW, the SW X-ray feature might be its star formation wake. That feature is about 18% as luminous as SE in the passband of the *Chandra* High Resolution Camera (HRC), indicating that it has $L(2 - 10 \text{ keV}) = 2.1 \times 10^{42} \text{ erg s}^{-1}$ (Civano et al. 2010, 2012).

From § 3.1, the new VLA upper limit to the SFR at the location of the SW X-ray feature is $\text{SFR} < 17 \text{ M}_\odot \text{ yr}^{-1}$ for a Kroupa IMF. This corresponds to $L(2 - 10 \text{ keV}) < 8.5 \times 10^{40} \text{ erg s}^{-1}$ according to Ranalli et al. (2003), who use a Salpeter IMF. Even with this caveat of different IMFs, the X-ray emission from the SW feature is much too luminous to be driven by star formation. This points to the SW X-ray feature being AGN-driven, perhaps, as Civano et al. (2012) suggest, because SE photoionizes the ambient ISM on kiloparsec scales and produces optical and X-ray emission lines analogous to the situation at radii beyond $2''$ (130 pc) in NGC 4151 (Wang et al. 2011b). Notably, SE's [OIII] $\lambda 5007$ luminosity is about 37-76 times that of NGC 4151 on kpc scales (Ho & Ulvestad 2001), perhaps because of SE's location in a merger remnant rather than in a typical LLAGN host.

3.3. The NW Optical Nucleus

The new VLA and VLBA nondetections of NW imply that any AGN-driven emission has K-corrected luminosities $\nu L_\nu(9.0 \text{ GHz}) < 6.6 \times 10^{38} \text{ erg s}^{-1}$ (3σ) on scales below 1.6 kpc and $\nu L_\nu(1.52 \text{ GHz}) < 4.7 \times 10^{38} \text{ erg s}^{-1}$ (6σ) on scales below 75 pc. From § 3.1, the luminosity of any AGN-driven emission from NW cannot exceed $\nu L_\nu(1.4 \text{ GHz}) = 6 \times 10^{38} \text{ erg s}^{-1}$. From § 3.1, the [O III] $\lambda 5007$ luminosity of NW is $L([\text{O III}]) = 4.8 - 9.9 \times 10^{42} \text{ erg s}^{-1}$ (Comerford et al. 2009b). The VLBA luminosity, free from contamination from star formation, thus implies that NW is radio quiet following the Zakamska et al. (2004) definition. The X-ray emission from the NW optical nucleus is less than 4.5% as luminous as SE in the HRC passband, suggesting that NW has $L(2 - 10 \text{ keV}) < 5.1 \times 10^{41} \text{ erg s}^{-1}$ (Civano et al. 2010, 2012).

The NW optical nucleus could harbor an intrinsically faint AGN, with a narrow emission-line region only. However, evidence for a very obscured Type 2 AGN in NW is beginning to emerge. Recent prescriptions for identifying obscured AGNs (Juneau et al. 2011) can be applied. From § 3.1, the excitation ratio of NW is $[\text{OIII}]\lambda 5007/\text{H}\beta = 3.4 - 4.4$ (Comerford et al. 2009b). Such a ratio, when combined with estimates for the host galaxy's stellar mass $M_\star \sim 10^{10-11} \text{ M}_\odot$ (Civano et al. 2010; Kartaltepe et al. 2010), occupy the AGN locus of the mass-excitation diagram (Fig. 4; Juneau et al. 2011). Moreover, as Civano et al. (2012) suggest, NW could lack an X-ray counterpart due to atomic absorption. Comparing NW's Compton-thickness parameter $T = L(2 - 10 \text{ keV})/L([\text{OIII}])$ to its [O III] $\lambda 5007$ luminosity (Comerford et al. 2009b; Civano et al. 2012) identifies it as a Compton-thick candidate (Fig. 10; Juneau et al. 2011).

NW could also lack a counterpart at $\nu = 9.0 \text{ GHz}$ due to free-free absorption by its narrow emission-line gas, a concept applied to account for the flat radio spectra of some Type 2 AGN with $L([\text{OIII}]) = 10^{42} \text{ erg s}^{-1}$ (Lal & Ho 2010). For a characteristic electron temperature $T_e = 10^4 \text{ K}$ and density $n_e = 10^3 \text{ cm}^{-3}$, a path length of about 380 pc gives a free-free optical depth of unity at $\nu = 10 \text{ GHz}$ (Ulvestad & Ho 2001). Intriguingly, this free-free path length resembles the scale length of about 100 mas (500 pc) reported for NW's starlight (Civano et al. 2010). This path length can be cross-checked in several ways. First, the $\text{H}\beta$ luminosity for either the blueshifted or redshifted narrow emission-line gas (Comerford et al. 2009b) shouldn't be exceeded; this can be achieved by invoking a plausible volume-filling factor $f \sim 1 - 3 \times 10^{-3}$. Second, if the narrow emission-line gas has a spherical geometry with diameter 150 mas ($2 \times 380 \text{ pc}$), the source at $\nu = 9.0 \text{ GHz}$ should be much smaller; this can be checked with sensitive VLBA imaging. Third, at VLBA resolutions the spectrum of the source at frequencies $\nu < 9.0 \text{ GHz}$ should be exponentially suppressed; this is also testable with sensitive VLBA imaging.

Civano et al. (2012) assembled the spectral energy distribution at far-infrared and shorter wavelengths, corrected it for the contributions of the Type 1 AGN in SE, and inferred an infrared (IR) luminosity $L(\text{IR}) \sim 6 \times 10^{44} \text{ erg s}^{-1}$. That luminosity corresponds to a Kroupa-based $\text{SFR} \sim 23 \text{ M}_\odot \text{ yr}^{-1}$ (Murphy et al. 2011, eqn. 4), although this value would be overestimated if dust warmed by an obscured Type 2 AGN in NW contributed to the IR luminosity (e.g., de Grijs et al. 1992; Juneau et al. 2013). From § 3.1, the new VLA upper limit to the SFR at the location of the NW optical nucleus is $\text{SFR} < 17 \text{ M}_\odot \text{ yr}^{-1}$. This lower radio-based SFR suggests that the IR photometry could suffer some contamination from dust warmed by an obscured AGN.

4. SUMMARY AND CONCLUSIONS

We presented new radio imaging of J1000+0206, a merger remnant at $z = 0.36$ with two optical nuclei, NW and SE, offset by 500 mas (2.5 kpc). The new VLA imaging at $\nu = 9.0 \text{ GHz}$ is sensitive to emission driven by AGNs and/or star formation, and the new VLBA imaging at $\nu = 1.52 \text{ GHz}$ is sensitive only to emission driven by AGNs. No radio emission was detected at these fre-

quencies. Combining new and prior results, the following self-consistent picture emerged:

- The new VLA photometry at $\nu = 9.0$ GHz implies a SFR $< 17 M_{\odot} \text{ yr}^{-1}$ for the inner merger remnant, the optical nuclei SE and NW, and the X-ray feature adjacent to the SE nucleus. After correcting the prior VLA photometry at $\nu = 1.4$ GHz for this SFR, the AGN-driven emission has an integrated luminosity $\nu L_{\nu}(1.4 \text{ GHz}) = (3 - 6) \times 10^{38} \text{ erg s}^{-1}$, in the realm of LLAGN in the local Universe.
- The properties of SE and its adjacent X-ray feature match those of the unobscured prototype AGN in NGC 4151. However, the luminosity of the narrow emission-line gas associated with SE is about forty to eighty times higher than that associated with the AGN in NGC 4151. Deeper radio, optical and X-ray studies of SE will test its resemblance to, and difference from, the Type 1 AGN prototype in NGC 4151. For example, the difference in narrow emission-line luminosities could reflect atypical, merger-induced conditions near SE.
- The properties of NW are consistent with it hosting a Compton-thick AGN that warms the ambient dust and photoionizes the narrow emission-line gas, and is free-free absorbed by that gas at $\nu = 9.0$ GHz. These findings enhance the prospects that AGN-driven emission could emerge from radio and X-ray studies of NW at deeper levels and X-ray studies of NW at harder wavelengths. For example, deeper VLBA imaging could reveal a radio spectrum that is exponentially suppressed by free-free absorption. These findings also underscore the urgency of localizing narrow emission-line gas, whether blueshifted or redshifted, to NW.

In the scenario where SE is an AGN that has recoiled from NW due to the asymmetric emission of gravitational waves during black-hole coalescence, NW cannot host an obscured AGN. The emerging evidence for a very obscured Type 2 AGN in NW thus both weakens the case for SE being a gravitational-wave recoil and strengthens the case that each optical nucleus contains its own AGN. Two interpretations are consistent with the latter scenario: (i) SE and NW mark inspiralling dual AGNs like those sought in systematic spectroscopic surveys for dual AGN candidates (Comerford et al. 2009a; Wang et al. 2009; Liu et al. 2010; Smith et al. 2010; Koss et al. 2012; Barrows et al. 2013; Comerford et al. 2013), or (ii) SE is a gravitational-slingshot recoil moving away from NW and the Type 2 AGN that it harbors (Civano et al. 2010, 2012; Blecha et al. 2013a).

It must be noted that SE's broad $H\beta$ emission line is redshifted by more than 1000 km s^{-1} relative to the narrow $H\beta$ emission line (Civano et al. 2010). Such large velocity offsets occur in less than 1 % of normal Type 1 AGN (Bonning et al. 2007; Eracleous et al. 2012), making it very unlikely that they will occur by chance in an inspiralling Type 1 AGN. In contrast, such large velocity offsets are predicted for a gravitational-slingshot recoil (Hoffman & Loeb 2007), a point in favor of that interpretation for J1000+0206.

We thank the referee for a timely and helpful report. We also acknowledge using Ned Wright's Cosmology Calculator (Wright 2006) and benefiting from helpful discussions with Michael Cooper, Francisco Muller-Sanchez, Jonathan Trump and Craig Walker. EM acknowledges financial support from the Deutsche Forschungsgemeinschaft through project FOR1254.

Facilities: VLA, VLBA.

REFERENCES

- Amaro-Seoane, P., Sesana, A., Hoffman, L., et al. 2010, *MNRAS*, 402, 2308
- Barrows, R.S., Sandberg Lacy, C.H., Kennefick J., et al. 2013, *ApJ*, 769, 95
- Blecha, L., Cox, T.J., Loeb, A., & Hernquist, L. 2011, *MNRAS*, 412, 2154
- Blecha, L., Civano, F., Elvis, M., & Loeb, A. 2013a, *MNRAS*, 428, 1341
- Blecha, L., Loeb, A., & Narayan, R. 2013b, *MNRAS*, 429, 2594
- Beswick, R.J., Pedlar, A., Mundell, C.G., & Gallimore, J.F. 2001, *MNRAS*, 325, 151
- Bonning, E.W., Shields, G.A., & Salvander, S. 2007, *ApJ*, 666, L13
- Calzetti, D. 2012, arXiv:1208.2991v1
- Civano, F., Elvis, M., Lanzuisi, G., et al. 2010, *ApJ*, 717, 209
- Civano, F., Elvis, M., Lanzuisi, G., et al. 2012, *ApJ*, 752, 49
- Comerford, J.M., Gerke, B.F., Newman, J.A., et al. 2009a, *ApJ*, 698, 956
- Comerford, J.M., Griffith, R.L., Gerke, B.F., et al. 2009b, *ApJ*, 702, L82
- Comerford, J.M., Pooley, D., Gerke, B.F., & Madejski, G.M. 2011, *ApJ*, 737, L19
- Comerford, J.M., Gerke, B.F., Stern, D., et al. 2012, *ApJ*, 753, 42
- Comerford, J.M., Schluns, K., Greene, J.E., & Cool, R.J. 2013, *ApJ*, in press, arXiv:1309.2284v1
- Condon, J.J. 1992, *ARA&A*, 30, 575
- Condon, J.J., Kellermann, K.I., Kimball, A.E., & Perley, R.A. 2013, *ApJ*, 768, 37
- de Grijp, M.H.K., Keel, W.C., Miley, G.K., Goudfrooij, & Lub, J. 1992, *A&AS*, 96, 389
- de La Fuente Marcos, R. & de La Fuente Marcos, C. 2008, *ApJ*, 677, L47
- Deller, A.T., Briske, W.F., Phillips, C.J., et al. 2011, *PASP*, 123, 275
- Dotti, M., Sesana, A., & Decarli, R. 2012, *Advances in Astronomy*, 940568
- Elvis, M., *BAAS*, 41, 708
- Eracleous, M., Boroson, T.A., Halpern, J.P., & Liu, J. 2012, *ApJS*, 201, 23
- Fu, H., Myers, A.D., Djorgovski, S.G., & Lin, Y. 2011a, *ApJ*, 733, 103
- Fu, Z. Zhang, Assef, R.J., et al. 2011b, *ApJ*, 740, L44
- Fu, H., Lin, Y., Myers, A.D., et al. 2012, *ApJ*, 745, 67
- Gallimore, J.F., & Beswick, R. 2004, *AJ*, 127, 239
- Garrett, M.A., Wrobel, J.M., & Morganti, R. 2005, *ApJ*, 619, 105
- Greisen, E.W. 2003, in *Information Handling in Astronomy*, ed. A. Heck (Dordrecht: Kluwer), 109
- Guedes, J., Madau, P., Mayer, L., & Callegari, S. 2011, *ApJ*, 729, 125
- Ho, L.C. 2008, *ARA&A*, 46, 475
- Ho, L.C. 2009, *ApJ*, 699, 626
- Ho, L.C., & Ulvestad, J.S. 2001, *ApJS*, 133, 77
- Hobbs, G., Archibald, A., Arzoumanian, Z., et al. 2010, *Class. Quantum Grav.*, 27, 084013
- Hoffman, L. & Loeb, A. 2007, *MNRAS*, 377, 957
- Juneau, S., Dickinson, M., Alexander, D.M., & Salim, S. 2011, *ApJ*, 736, 104
- Juneau, S., Dickinson, M., Bournaud, F., et al. 2013, *ApJ*, 764, 176

- Kartaltepe, J.S., Sanders, D.B., Le Floch, E., et al. 2010, *ApJ*, 721, 98
- Kim, M., Ho, L.C., & Im, M. 2006, *ApJ*, 642, 702
- Komassa, S., Burwitz, V., Hasinger, G., et al. 2003, *ApJ*, 582, L15
- Koss, M., Mushotzky, R., Teiester, et al. 2012, *ApJ*, 746, L22
- Kukula, M., Pedlar, A., Baum, S.A., & O’Dea, C.P. 1995, *MNRAS*, 276, 1262
- Kulkarni, G. & Loeb, A. 2012, *MNRAS*, 422, 1306
- Lal, D.V., & Ho, L.C. 2010, *AJ*, 139, 1089
- Lilly, S.J., Le Fevre, O., Renzini, A., et al. 2007, *ApJS*, 172, 70
- Liu, X., Shen, Y., Strauss, M.A., & Greene, J.E. 2010, *ApJ*, 708, 427
- Liu, X., Shen, Y., & Strauss, M.A. 2012, *ApJ*, 745, 94
- McMullin, J. P., Waters, B., Schiebel, D., Young, W., & Golap, K. 2007, *Astronomical Data Analysis Software and Systems XVI* (ASP Conf. Ser. 376), ed. R. A. Shaw, F. Hill, & D. J. Bell (San Francisco, CA: ASP), 127
- Middelberg, E., Deller, A.T., Norris, R.P., et al. 2013, *Å*, 551, A97
- Mundell, C.G., Wrobel, J.M., Pedlar, A., & Gallimore, J.F. 2003, *ApJ*, 583, 192
- Murphy, E.J., Condon, J.J., Schinnerer, E., et al. 2011, *ApJ*, 737, 67
- Napier, P.J., Bagri, D.S., Clark, B.G., et al. 1994, *Proc. IEEE*, 82, 658
- Owen, F.N., O’Dea, C.P., Inoue, M., & Eilek, J.A. 1985, *ApJ*, 294, L85
- Perley, R. A., Chandler, C. J., Butler, B. J., & Wrobel, J. M. 2011, *ApJ*, 739, L1
- Perley, R. A., & Butler, B. J. 2013, *ApJS*, 204, 19
- Ranalli, P., Comastri, A., & Setti, G. 2003, *Å*, 399, 39
- Rosario, D.J., Shields, G.A., Taylor, G.B., et al. 2010, *ApJ*, 716, 131
- Schinnerer, E., Smolcic, V., Carilli, C., et al. 2007, *ApJS*, 172, 46
- Schinnerer, E., Sargent, M.T., Bondi, M., et al. 2010, *ApJS*, 188, 384
- Scoville, N., Abraham, R.G., Aussel, H., et al. 2007, *ApJS*, 172, 38
- Shen, Y., Liu, X., Greene, J.E., & Strauss, M.A. 2011, *ApJ*, 735, 48
- Smith, K.L., Shields, G.A., Bonning, E.W., et al. 2010, *ApJ*, 716, 866
- Smolcic, V., Schinnerer, E., Scodegion, M., et al. 2008, *ApJS*, 177, 14
- Terashima, Y., & Wilson, A.S. 2003, *ApJ*, 583, 145
- Trump, J.R., Impey, C.D., Kelly, B.C., et al. 2009, *ApJ*, 700, 49
- Trump, J.R., Impey, C.D., Kelly, B.C., et al. 2011, *ApJ*, 733, 60
- Trump, J.R., Impey, C.D., Kelly, B.C., et al. 2013, *erratum*
- Ulvstad, J.S., & Ho, L.C. 2001, *ApJ*, 558, 561
- Van Wassenhove, S., Volonteri, M., Mayer, L., et al. 2012, *ApJ*, 748, L7
- Wang, J., Chen, Y., Hu, C., Mao, W., & Bian, W. 2009, *ApJ*, 705, L76
- Wang, J., Fabbiano, G., Elvis, M., et al. 2011a, *ApJ*, 736, 62
- Wang, J., Fabbiano, G., Elvis, M., et al. 2011b, *ApJ*, 742, 23
- Wright, E.L. 2006, *PASP*, 118, 1711
- Zakamska, N.L., Strauss, M.A., Heckman, T.M., Ivezić, Z., & Krolick, J.H. 2004, *AJ*, 128, 1002